2013 IEEE International Conference on Robotics and Automation (ICRA)
Karlsruhe, Germany, May 6-10, 2013

Estimating attitude and wind velocity using biomimetic sensors on a microrobotic bee

Sawyer B. Fuller, Alexander Sands, Andreas Haggerty, Michael Karpelson, and Robert J. Wood

Abstract— **This paper discusses recent developments in sensors for the Harvard RoboBee. The RoboBee is a sub-100 mg flapping-wing micro-aerial vehicle that is able to lift its own weight under external power, but, like flying insects, is unstable in flight without active feedback. We discuss design and characterization of two low-latency insect-inspired sensors for flight control: an antenna to sense airspeed and light-sensing ocelli to estimate attitude angle relative to a luminous sky. We demonstrate accurate wind velocity estimation in a wind tunnel despite the effect of nearby flapping wings. We also demonstrate pitch angle control using the ocelli on a wire-mounted RoboBee that is free to rotate about its pitch axis. These flight-weight sensors are essential first steps toward autonomous upright stability and controlled forward motions.**

I. Introduction

The Harvard RoboBee is a sub-100 mg micro-aerial vehicle (MAV), the first insect-sized robot able to take off and lift its own weight [1]. Developing this vehicle into an autonomous vehicle is motivated by its possible applications in search and rescue and assisted agriculture, as well as the unique engineering challenges it poses. Machine elements such as motors, bearings, and airfoils become inefficient as they get smaller due to the physics of scaling: surface effects increasingly dominate Newtonian forces [2] and viscous forces dominate lift-generating aerodynamic inertial forces [3]. Hence, novel solutions are required for nearly every component. We take inspiration from flying insects, whose superlative aerobatic agility rivals any man-made flying vehicle [4]. Accordingly, our vehicle uses muscle-like piezoelectric actuators to generate forces, flexures for articulation, and harnesses unsteady aerodynamic forces by flapping its wings with a passive hinge joint [5], [6]. We have demonstrated constrained liftoff [5], vertical position control [7], and near-hover using passive air dampers [8] of the Harvard RoboBee using these techniques. Attaining free-flight stability, however, is an area of active research.

Fast, lightweight proprioceptive sensors are a necessary component for autonomous stability and they may be essential for recreating the fast maneuvers that have been observed in biological insects [9]. Previous results have proposed a number of sensors that could be integrated into such a vehicle [10], [11], [12], but have not demonstrated their operation on insect-scale robots. In this work we consider two such high-bandwidth sensors: a biomimetic ocelli and a biomimetic antenna, and demonstrate both sensors in operation on a flapping-wing RoboBee. We discuss their fabrication, characterization, and how they could be used to stabilize and control flight motions of the RoboBee.

The authors are with the School of Engineering and Applied Sciences, Harvard University, Cambridge MA 02138 USA and the Wyss Institute for Biologically Inspired Engineering, Harvard University, Boston, MA 02115, USA (E-mail: minster@seas.harvard.edu, rjwood@seas.harvard.edu)

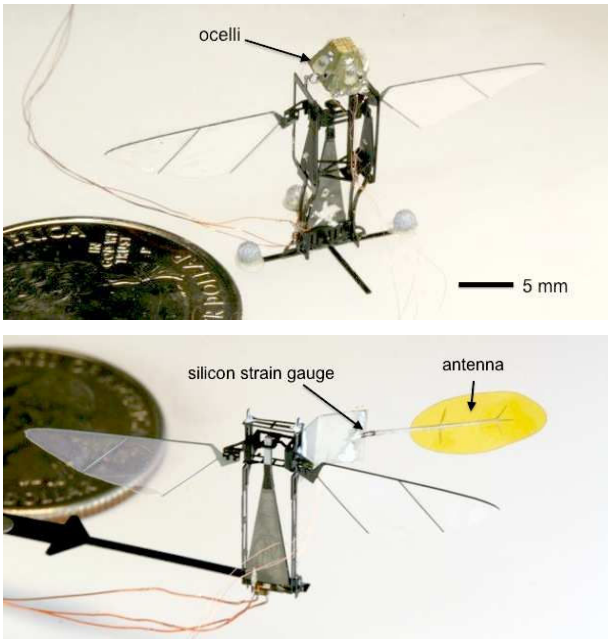

Fig. 1. Harvard RoboBee prototypes with biomimetic sensors. (top) A bee with biomimetic ocelli (pyramidal structure at top) senses light levels with four phototransistors to estimate the angle orientation relative to vertical. (bottom) Bee with a single biomimetic antennae (yellow paddle-shaped device extending laterally to right) for fast feedback of wind velocity. A pair of silicon strain gauges are adhered to the base of the antenna structure. A U. S. quarter dollar coin is shown for scale.

II. Biomimetic Ocelli

Almost all insects have three light sensors, distinct from the compound eyes, that point roughly upward and sense the sky and/or the sun. These three sensors are relatively defocused and carry many neurons that sample the same defocused light information [13]. They thus capture much more light than do the compound eyes, and this is thought to allow them to quickly sense changes to aid in rapid self-righting maneuvers [14].

A. Design and fabrication

We took cues from insect ocelli for the design of our biomimetic ocelli, so they have a superficial resemblance.

978-1-4673-5642-8/13/$31.00 ©2013 IEEE

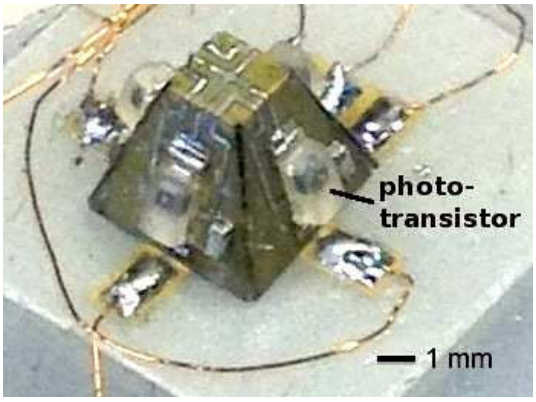

Fig. 2. The biomimetic ocelli consists of four phototransistors packaged in a clear plastic diffuser. These are soldered to a circuit board that is then folded into a pyramid shape.

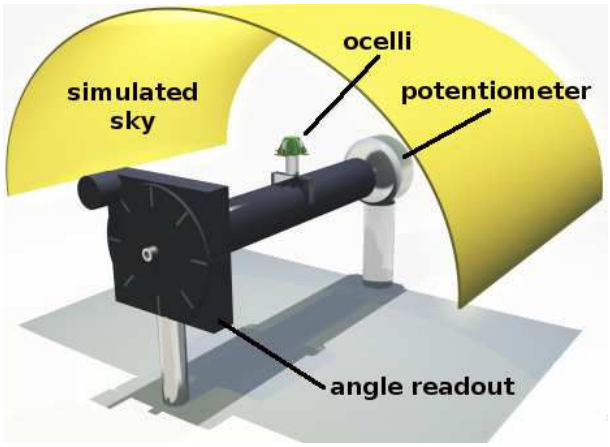

Fig. 3. Calibrating the biomimetic ocelli. A light diffuser made of a 250 μm thick translucent sheet of fiberglass (yellow) provided uniform, sky-like illumination. To calibrate, the ocelli prototype (small green pyramidal structure at center) was attached to an axle and made to rotate while both its tilt angle and light readings from the phototransistors were recorded by a data acquisition system. The dimensions of the virtual sky in the calibration apparatus are approximately 25x25 cm.

Our ocelli increases the number of sensors to four for simplicity of control design [10], but retains the $\approx 180°$ defocused light acceptance angle and 30° inclination away from the horizontal as observed in flies [15].

The basic structure of the device is formed by a lightweight folded circuit board. Traces were fabricated by laser-ablating the copper layer of copper-clad polyimide. Subsequently, the outline of the board was cut by laser and a unidirectional carbon fiber layer was adhered to the back to increase structural stiffness. Surface-mount components were soldered on by hand, and the pyramid structure was then hand-folded into shape. Each of the four light detectors consists of an OSRAM SFH3010 phototransistor and a 2 MΩ resistor in a common-emitter configuration with a supply voltage of 10V. The voltage reading is taken from the collector of each transistor and rises with increasing luminance. The device weighs 21 milligrams and measures 4×4×3.3 mm (Figure 2).

B. Characterization and calibration

We designed our attitude estimation algorithm to operate from input from a large-field "sky" input, rather than a point light source as described in [10], because the lighting of our multi-camera free-flight motion capture arena consists of bright infrared lights emitting from each camera. Indoor lighting also typically consists of an array of overhead lights. For the defocused phototransistors, this array of point light sources is more like a diffuse sky than a single point source of light. In the calibration and control experiments described in this work, we built a small virtual "sky" to approximate this light field. To calibrate, we attached the ocelli device to a rotating axle whose position was measured by a calibrated potentiometer (Figure 3).

We took measurements of the ocelli response to a number of different lighting conditions to ensure that the measurement was robust to such variations. For example, lighting would be expected to change dramatically when flying from indoors to outdoors. The bee would be expected to operate correctly in both environments. Recordings from different lighting conditions are shown in Figure 4. If the phototransistors are not saturated, the voltage readout is a smooth function of tilt angle, suggesting a possible method to estimate tilt angle from the two phototransistor voltages.

The next step was to estimate the pitch angle from these luminance readings. Because our design specification was that the ocelli function in a range of different lighting conditions, we normalized brightness. If O_1 and O_2 are ocelli voltages from an opposing pair of phototransistors whose angle we would like to estimate, we normalized by the mean of the two voltages, $\overline{O} = \frac{1}{2}(O_1 + O_2)$, according to

$$\begin{aligned} O_{1n} &= \frac{O_1}{\overline{O}} \\ O_{2n} &= \frac{O_2}{\overline{O}}. \end{aligned}$$

The difference of these two is the signal,

$$O_d = O_{1n} - O_{2n}.$$

This value is a roughly monotonic function of angle for our desired operating range of $\pm 45°$. We performed a fifth-order polynomial fit of O_d to pitch angle using the MATLAB command polyfit. Thus, estimating pitch angle only requires evaluating a polynomial, imposing minimal computational requirements for a realtime controller. Results of the calibration are shown in Figure 5. Different brightnesses have almost no effect on the angle estimate, whereas the estimate is changed by changing the pattern of light. With one exception, the point light trial, the estimate is smooth, permitting its use in a pitch angle feedback controller. The slopes are not the same, but we rely on the robustness of our feedback controller to gain uncertainty to permit stable operation despite this variability.

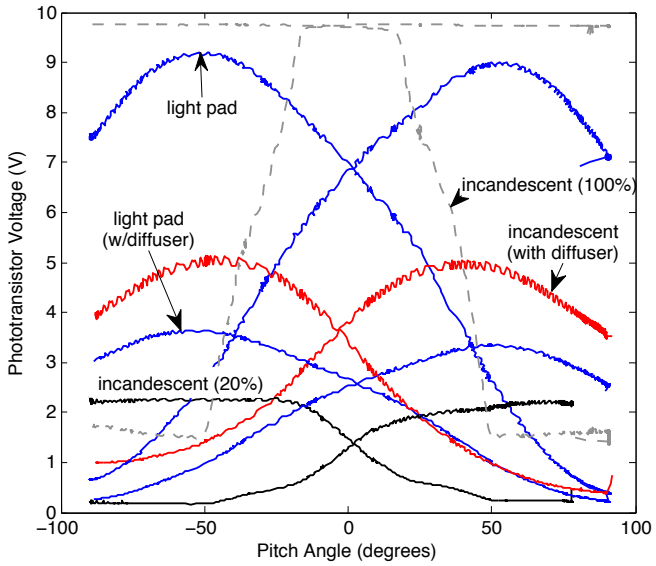

Fig. 4. Voltage recordings from an opposing pair of ocelli phototransistors as the device is slowly rotated through 180° by hand with and without a diffusing sky as shown in Figure 3. "Light pad" denotes that illumination was provided by a pair of 10 cm × 10 cm fluorescent illumination panels mounted 10 cm above the diffuser. In one trial, a secondary diffuser was added to assess the response in dim light. "Incandescent" was a variable-brightness fiber-optic light mounted 50 cm directly above the ocelli. We show the responses to an intermediate brightness setting and the diffuser, as well as with no diffuser to illustrate the response properties of the phototransistor to a point light source. At low brightness, the phototransistors exhibit a response profile to a point light source that is approximately flat over a 120° range. At high brightness, the phototransistors saturate and produce a constant 10V signal (dashed traces), impairing the ability to estimate angles. The small oscillation in the signal is due to 60 Hz AC line noise.

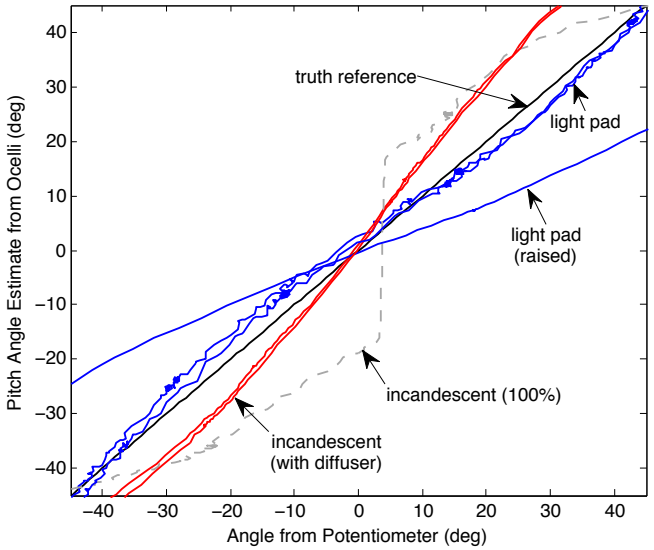

Fig. 5. The calibrated ocelli angle estimate vs. true angle. All estimates are based on a calibration to the "light pad" condition plotted in Figure 4. The results demonstrate capability to estimate pitch angle despite the effect of different brightnesses and lighting conditions as described in Figure 4. The two incandescent and two light pad trials show how the estimate changes with a change in brightness. "Raised" shows how the estimate is changed under the same lighting conditions as the light pad condition, but with the virtual sky raised by 5 cm. The raised sky condition was added to simulate the visual effect of changing the height of the virtual sky as would occur for a RoboBee in free flight if it were to change altitude in an enclosed space. Though the slope is not identical for all cases, it is smooth, meaning it can be used for feedback control. The feedback controller was designed to be robust to such small changes in gain. The condition of full-brightness incandescent is shown to give an example of a failure mode, though our system was not designed to operate correctly for this condition.

C. Pitch angle control

With a rise time on the order of 10 μs, the phototransistors provide a bandwidth far in excess of the speed of dynamics of our RoboBee, so the estimate can be approximated as instantaneous. Given the fast estimate of pitch angle using an opposing pair of angled phototransistors from the ocelli, we designed a feedback control loop in which the bee could maintain a desired pitch angle. We attached the ocelli to the anterior of the bee with as shown in Figure 1 and placed it in the virtual sky arena. Similar to the pitch control experiment of [16], we mounted the bee on a thin wire so that its pitch angle axis was free to rotate while all other degrees of freedom were constrained (Figure 6). The basic design of the feedback system is pictured in Figure 7. The controller was executed on a PC running the XPC Target software environment (Mathworks, Newton, MA, USA). Using a digital-to-analog converter board, the controller generated an analog voltage signal, amplified by a high-voltage amplifier, that drove the bee's piezoelectric actuator to flap the wings at 100 Hz with a fixed 220V amplitude. Pitch torque was applied by altering the mean stroke position of the wings by changing the mean voltage of the sinusoid driving signal [17].

To design the controller, we used the conversion factor from mean wing voltage to pitch torque from [17] and esti-

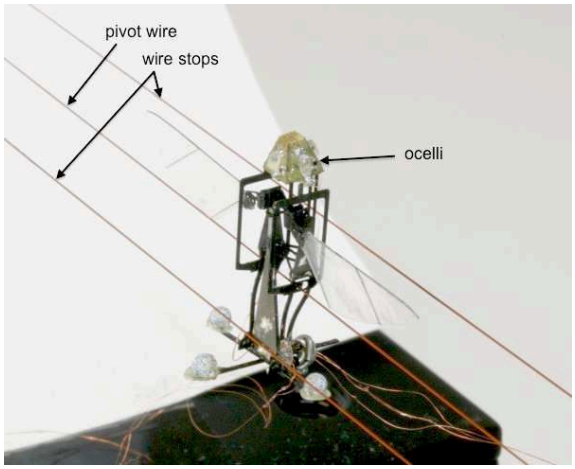

Fig. 6. RoboBee with ocelli attached to a thin wire (middle wire) near its center of mass so that only its pitch angle degree of freedom was unconstrained. The outside pair of wires limits the extent of rotation to avoid wire tangles.

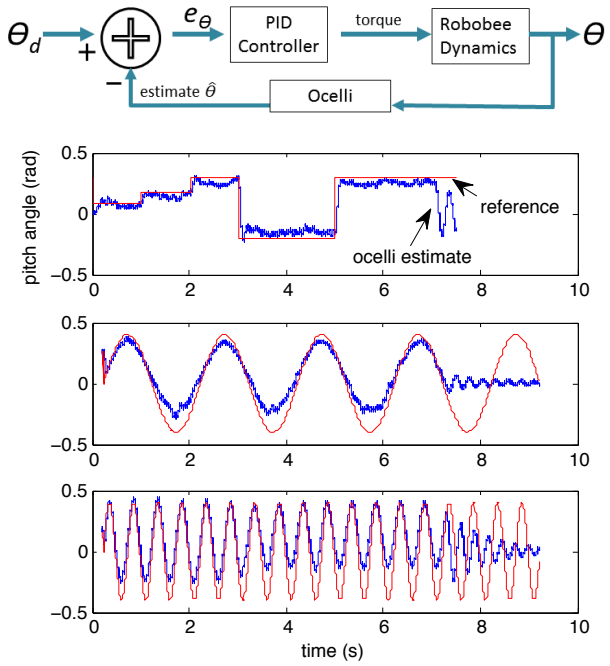

Fig. 7. Pitch control of the RoboBee suspended on a wire for single-axis rotational freedom. (top) A feedback diagram shows how the bee feeds its estimate of pitch angle taken from the ocelli into a PD controller which in turn calculates mean-stroke-position commands to flap the wings. (middle and bottom) The bee can follow commanded trajectories (red), with a step response time of approximately 100 ms. Errors are larger for large excursions because the restoring torque of the counterweight increases as the angle moves away from zero. The oscillations near the end of each of the trials occur after the controller and wings are turned off and show the bee's natural damped dynamics as it pivots around its mounting wire. At around 3 s in the bottom trial, the left wing failed and detached, reducing the available torque and leading to greater error at negative pitch angles.

mated the rotational moment of inertia of the vehicle using a computer model in SolidWorks. For ease of experiment, we mounted a small weight made of solder to the bottom of the bee so that its neutral position was upright, and accounted for this weight in the model. Using the model, we designed a proportional-derivative controller using the python-control library (`http://python-control.sf.net`) that provided rotational damping using the derivative term. Pitch torque was generated by altering the mean stroke angle, a mechanism that is thought to be used by insects to modulate pitch torque. The controller was able to drive the body angle to the desired setpoint as shown in Figure 7, with a short, $<$0.1 s ramp time. The results indicate that this sensor can provide a high-bandwidth pitch angle estimate that is usable for pitch angle control.

D. Future work

While we were able to use the ocelli to measure absolute angle, this may not be possible in more general settings. We found that when the light source or virtual horizon was tilted away from vertical, the estimate of the angle of the ocelli was tilted as well, as might intuitively be expected. A potential solution is to use the ocelli to only measure rate of change rather than absolute orientation the light source. An aerodynamic model of the RoboBee taken from wind tunnel tests [8] suggests that knowledge of the rotation rate may be sufficient to achieve upright stability. Because the center of mass of the bee is below the center of pressure of the wings, it is only necessary to apply a sufficiently large counter-torque proportional to the rate of rotation to insure upright stability. From the data of Figure 5, because the plot is smooth (with the exception of the point light source), its output could be differentiated in time, thus providing an estimate of rotation rate. By using the derivative, the problem of having the light source tilted relative to the bee is eliminated: a tilted light source shifts the plot laterally but does not change its derivative. Because the rate of change of lighting conditions due to lateral motion (such as when moving between rooms) is likely to be much slower than rotational dynamics, such "sensor disturbances" should not significantly affect stability. Though taking the derivative increases noise, our controller operated acceptably using a derivative term calculated as first-order difference, suggesting the problem is not insurmountable. Biological evidence seems to suggest the ocelli reflex is more derivative-like than proportional-like [13], supporting the view that this may be how ocelli are used by flying insects.

III. Biomimetic Wind Sensors

If autonomous upright stability can be achieved by using ocelli or passive air dampers [8], the next task is to translate in space. In a typical scenario, the RoboBee will fly in confined spaces, in which the GPS signal is either denied, or whose ~1m precision is insufficient for navigating through obstacles such as a doorway [18]. Taking inspiration from insects once again, it is likely that RoboBee navigation will rely heavily on optic flow [19]. However, estimating self-motion with optic flow has significant limitations. First, estimating optic flow requires a comparison of current visual input with a previous visual input [20], introducing a delay the control loop. Secondly, precise self motion estimation with vision requires significant computation power, taking as long as 2 minutes to compute for rovers on Mars [21], a problematic delay for a dynamic insect-sized robot. But perhaps the greatest challenge is that optic flow computation has limited precision, suffering from uncertainties that arise from the so-called "aperture problem" [20], as well varying in strength depending on the distance to obstacles (because it measures angular rate rather than linear rate of motion). Therefore, while providing rich information, vision is both a slow and uncertain speed sensor, which is problematic for a dynamic, flying robot that needs low-latency feedback to maneuver.

Turning to insects for inspiration, evidence has shown that many flying insects complement optic flow sensing from their eyes with a wind sense mediated by either bristles or the antennae [14], [22]. A fast wind sense could augment a slower optic flow based controller. One way of integrating these two sensors would be to operate a fast inner loop to regulate airspeed while an outer loop regulated groundspeed

using optic flow. Might such an architecture have the downside that the airspeed regulator would be heavily perturbed by changing wind conditions in the outdoors? Atmospheric wind is typically turbulent, and thus follows a $f^{-5/3}$ power spectral density in which low-frequency disturbances are much stronger than are those of high frequency [23]. Hence, though a fast airspeed sensor might increase sensitivity to fast wind transients, such transients are relatively weak. The more powerful wind disturbances at lower frequency, however, are slow enough to be adequately rejected by a slower visual control loop.

Our goal is to design a low-mass wind sensor to mount on the RoboBee to sense airspeed to eventually be incorporated into such an architecture. We again took inspiration from flies. Flies sense wind using their antennae by extending a paddle-like organ, the arista, laterally away from the head, so that it is subject to wind-induced deflection. A sensitive organ at the base of the cantilevered antenna senses strain changes [24]. In a similar fashion, our design uses a pair of silicon microfabricated strain gauges on either side of a thin, compliant beam attached to a paddle structure. We tested the antenna prototypes in a low-speed wind tunnel (Engineering Laboratory Design, Inc., Model 40), amplifying the output of the strain gauge in a Wheatstone Bridge circuit configuration with an operational amplifier at 1500× gain (AD623). For calibration, we set the wind tunnel to a desired speed, waited for the wind velocity to stabilize (approximately 30 seconds), and then recorded voltage data using a National Instruments USB digital-to-analog converter.

Our antenna fabrication effort differs from prior work [25], [26] in that we used the same fabrication technology used to construct the body of the RoboBee. By leveraging these techniques, the antenna could be integrated into our layered monolithic fabrication process [27] in future RoboBee designs. The part was cut using an ultraviolet-wavelength laser, which provides a 10 μm spot size and ~1 μm repeatability, and can cut virtually any thin material including metals and carbon fiber.

In the prototyping phase we experimented with a number of materials including fiberglass, carbon fiber, polyimide, and steel. We found that it was critical to choose the beam stiffness appropriately. Too stiff and the voltage response of the of the gauge bridge remains below the noise floor; too flexible and residual strains from fabrication lead to a non-monotonic voltage response as a function of wind speed, making it impossible to estimate wind strength based on voltage output from the bridge. Our final design, made of 25 μm and steel, produced a monotonic response and had sufficient flexibility to deflect under the induced forces of the wind in the 0 to 2 m/s range expected of our RoboBee (Figure 10). The semiconductor strain gauges (Micron Instruments, Simi Valley, CA, USA "U-gauge" model SS-060-033-300 measuring 1.5 mm×0.4 mm×12μm thick) were bonded to the base of the antennae with cyanoacrylate glue. A flat polyimide "paddle" was attached with the same adhesive at the distal end to increase sensitivity. To avoid undesired

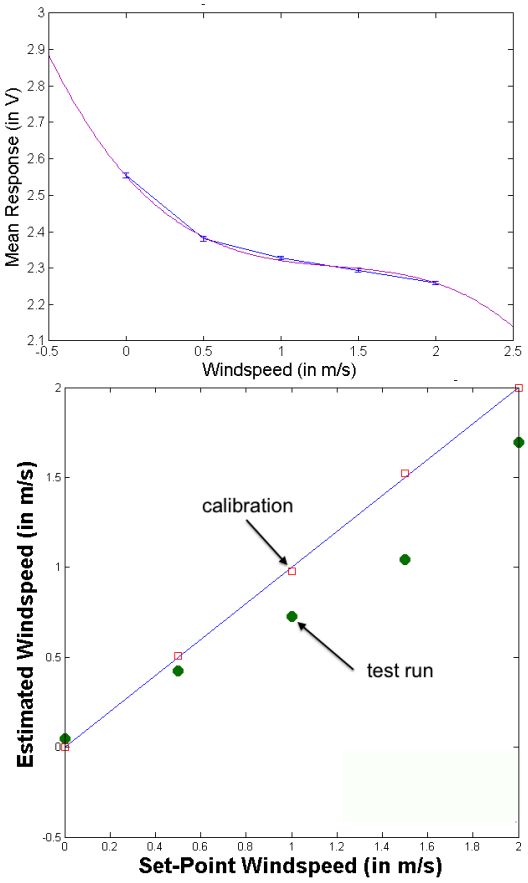

Fig. 8. Calibration of the biomimetic antenna wind sensor. (top) Measured voltage output of the Wheatstone bridge circuit after amplification and polynomial calibration fit; (bottom) voltage responses of two wind tunnel measurements on different days. Though the measurements are not perfectly repeatable, the variations are likely small enough that a feedback controller could be designed with sufficient robustness to ensure stability.

deflections in the polyimide paddle at high airspeed, we reinforced it with lightweight cross-beams cut out of the steel. The device is shown attached to the bee in Figure 1, and resembles the branching aristae of dipteran flies [24]. This device weighed approximately 18 mg, thus falling within our mass budget [28].

Test results from the wind tunnel are shown in Figure 8. From the response in this figure, we are able to distinguish small wind speeds below 0.5 m/s. A cubic polynomial fit the data well, allowing the calibration to be inverted to estimate airspeed (Figure 8). A second trial in which the antenna was removed and subsequently placed back in the wind tunnel gave an error of approximately 20 % relative to the first trial. Though the flow regime would be expected to apply a force that varies as the square of wind velocity, we hypothesize that response shape may not match this because of insufficient stiffness of the cyanoacrylate glue used to bond the strain gauges and the antenna base.

A. *Sensitivity to the influence of flapping and vibration*

Recent evidence has emerged that flies may sense the motion of their own wings using their antennae [29], which are

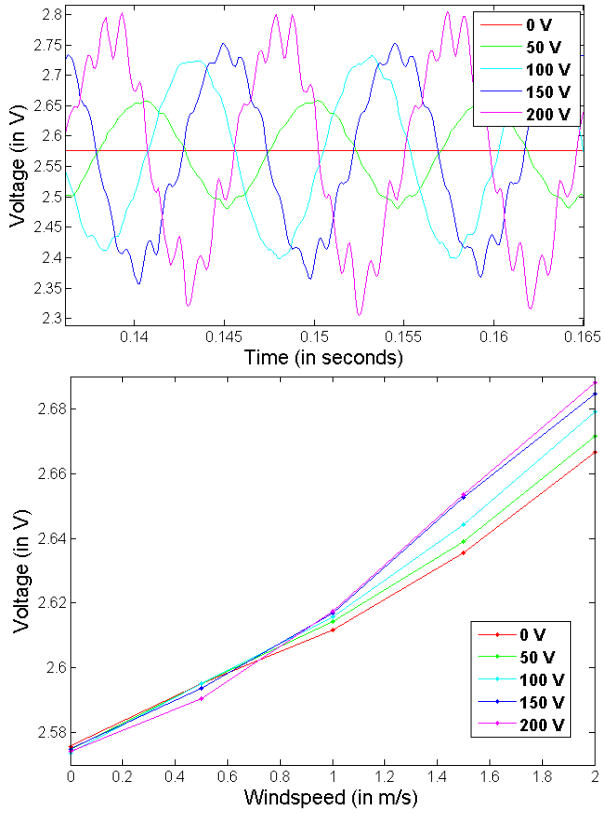

Fig. 9. Mean antenna voltage response when mounted on the bee is not dependent on wing flapping amplitude. (top) The amplitude of antenna oscillation grows with wing flapping amplitude, and also reveals a resonant mode at approximately 9× the flapping frequency. (bottom) Changes in flapping amplitude in the vicinity of the antenna does not significantly alter its mean voltage response, indicating it can sense wind velocity despite flapping and vibration disturbances.

particularly sensitive to vibrations at the flapping frequency [22]. An antenna that could detect the flapping motion of the wings could provide feedback about wing motion or wing damage. Alternatively, proximity to the wings or vibration of the airframe could compromise the ability to sense wind for flight control. To investigate these possible effects on our biomimetic antenna, we mounted it to the RoboBee in a position relative to the wings that mimicked its location on flies and measured its response to a range of different wing-flapping amplitudes and wind velocities. The results indicate first that the amplitude of measured oscillations at wingbeat does vary significantly with wingbeat amplitude. This information could be used to detect the level of performance of a wing actuator during calibration, or to detect wing damage, for example. Secondly, the mean deflection due to the force of the wind is not altered by this disturbance, indicating that the estimate of wind speed in the vicinity of flapping wings is not seriously compromised (Figure 9). In other words, the low-frequency component of the response of the antennae can provide an estimate of airspeed while a component at the flapping frequency could provide feedback about activity of the wings.

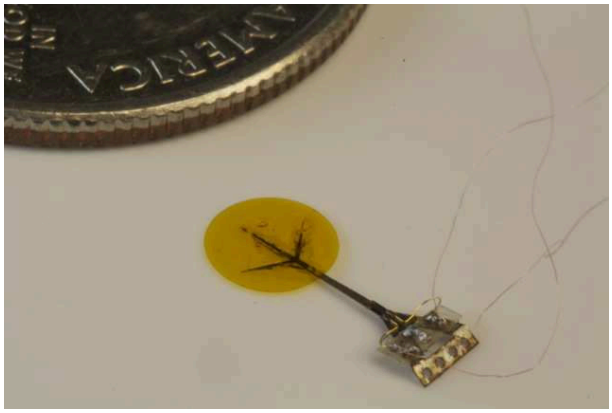

Fig. 10. Biomimetic antenna, shown with a U.S. Quarter Dollar coin for scale. The U-shaped silicon strain gauge is mounted at the base of the extension arm of the antenna. A second, identical strain gauge is mounted on the other side.

B. *Future work*

We believe the error between measurements shown in Figure 8 was due to small changes in resistance caused by deflection of of the 30 cm wires that connected the strain gauges to the amplifier. Local conditioning circuitry such as an onboard amplifier or buffer (e.g., Microchip model MCP6001T-I/LT, weighing ~5 mg), could eliminate this problem. To reduce weight, we designed and fabricated a next-generation antenna that is much smaller but similarly sensitive, by removing unnecessary material (Figure 10). This prototype has a mass of only 4 mg, suggesting it could be deployed in greater numbers across the bee as necessary for wind sensing.

IV. Conclusions

In this work we have demonstrated two insect-inspired sensors for the Harvard RoboBee: a wind-sensing antenna and a light-sensing ocelli.

The antenna was able to sense wind speeds down to ~0.1 m/s, and operated in spite of the confounding effect of nearby flapping wings and vibration, indicating that it should have sufficient sensitivity to work in a fast feedback loop to control airspeed in flight. Future work will attempt to reduce the size and mass without compromising sensitivity, so that they can be deployed in multiple places on the bee to sense local flow patterns or provide more information about the motion of the bee.

We demonstrated pitch angle control on a wire using the ocelli, an example of active feedback with an onboard sensor. The design and fabrication of the ocelli prototype reported here was necessary to reduce mass sufficiently to fall under the ~30 mg payload capacity of our bumblebee-sized robot. It is possible that a light-based sensor such as our ocelli may be able to estimate rotation rates with less noise than comparably-scaled MEMS rate gyros. Some small gyros have been reported to have significant sensitivity to the vibratory environment associated with flapping flight [30]

The authors believe these two sensors provide sufficient information to enable upright stability and controlled forward motions of the RoboBee. With the advent of recent prototypes that have the ability to impart torques around multiple axes [17], [31] and therefore the ability to actively stabilize and control flight motions, these sensors may thus represent the first possible set of sensors for performing autonomous flight. Moreover, their high bandwidth may also be essential to provide the fast feedback necessary for performing high-gain aggressive dynamic maneuvers.

V. Acknowledgements

The authors would like to thank Daniel Vogt, Pakpong Chirarattanon, and Mike Smith for valuable assistance during the preparation of this manuscript. This work was partially supported by the National Science Foundation (award numbers CCF-0926148 and CMMI-0746638) and the Wyss Institute for Biologically Inspired Engineering. Any opinions, findings, and conclusions or recommendations expressed in this material are those of the authors and do not necessarily reflect the views of the National Science Foundation

References

[1] Robert J. Wood, Ben Finio, Michael Karpelson, Kevin Ma, Nestor O. Pérez-Arancibia, Pratheev S. Sreetharan, Hiroto Tanaka, and John P. Whitney. Progress on "pico" air vehicles. *The International Journal of Robotics Research*, 31(11):1292–1302, 2012.

[2] W. S. N. Trimmer. Microbots and micromechanical systems. *Sensors and Actuators*, 19:267–287, 1989.

[3] U. Pesavento and Z.J. Wang. Flapping wing flight can save aerodynamic power compared to steady flight. *Physical review letters*, 103(11):118102, 2009.

[4] M. F. Land and T. S Collett. Chasing behavior of houseflies. *Journal of Comparative Physiology A*, 89:331–357, 1974.

[5] R. J. Wood. The first takeoff of a biologically inspired at-scale robotic insect. *IEEE Journal of Robotics and Automation*, 24(2):341–347, 2008.

[6] R. J. Wood, S. Avadhanula, M. Menon, and R. S. Fearing. Microrobotics using composite materials: the micromechanical flying insect thorax. In *Proc. IEEE Int. Conf. Robotics and Automation ICRA '03*, volume 2, pages 1842–1849, 2003.

[7] Néstor O Pérez-Arancibia, Kevin Y Ma, Kevin C Galloway, Jack D Greenberg, and Robert J Wood. First controlled vertical flight of a biologically inspired microrobot. *Bioinspiration and Biomimetics*, 6(3):036009, Sep 2011.

[8] Zhi Ern Teoh, Sawyer B. Fuller, Pakpong C. Chirarattananon, Nestor O. Perez-Arancibia, Jack D. Greenberg, and Robert J. Wood. A hovering flapping-wing microrobot with altitude control and passive upright stability. In *Proceedings of the IEEE/RSJ International Conference on Intelligent Robots and Systems (IROS)*, 2012.

[9] Gwyneth Card and Michael H. Dickinson. Performance trade-offs in the flight initiation of *Drosophila*. *The Journal of Experimental Biology*, 211:341–353, 2008.

[10] Wei-Chung Wu, L. Schenato, R. J. Wood, and R. S. Fearing. Biomimetic sensor suite for flight control of a micromechanical flying insect: design and experimental results. In *Proc. IEEE Int. Conf. Robotics and Automation ICRA '03*, volume 1, pages 1146–1151, 2003.

[11] W. C. Wu, R. J. Wood, and R. S. Fearing. Halteres for the micromechanical flying insect. In *In Proc of the IEEE Int?l Conf on Robotics and Automation*, pages 60–65, 2002.

[12] Xinyan Deng, L. Schenato, Wei Chung Wu, and S.S. Sastry. Flapping flight for biomimetic robotic insects: part I-system modeling. *Robotics, IEEE Transactions on*, 22(4):776 –788, aug. 2006.

[13] Roland Hengstenerg. *Multisensory control in insect oculomotor systems*, chapter Visual Motion and its role in the stabilization of gaze, pages 285–298. Elsevier Science Publishers, 1993.

[14] Graham K. Taylor and Holger G. Krapp. Sensory systems and flight stability: What do insects measure and why? In J. Casas and S.J. Simpson, editors, *Insect Mechanics and Control*, volume 34 of *Advances in Insect Physiology*, pages 231 – 316. Academic Press, 2007.

[15] H. Schuppe and Roland Hengstenberg. Optical properties of the ocelli of calliphora erythrocephala anmd their role in the dorsal light response. *Journal of Comparative Physiology A*, 173:143–149, 1993.

[16] Nestor O. Perez-Arancibia, Pakpong Chirarattananon, Benjamin M. Finio, and Robert J. Wood. Pitch-angle feedback control of a biologically inspired flapping-wing microrobot. In *International Conference on Robotics and Biomimetics*, 2011.

[17] B.M. Finio and R.J. Wood. Open-loop roll, pitch and yaw torques for a robotic bee. In *IEEE/RSJ Int. Conf. on Intelligent Robots and Systems*, 2012.

[18] Antoine Beyeler, Jean-Christophe Zufferey, and Dario Floreano. Vision-based control of near-obstacle flight. *Autonomous Robots*, 27:201–219, 2009. 10.1007/s10514-009-9139-6.

[19] P.-E. J Duhamel, N.O. Perez-Arancibia, G.L. Barrows, and R.J. Wood. Altitude feedback control of a flapping-wing microrobot using an on-board biologically inspired optical flow sensor. In *IEEE Int. Conf. on Robotics and Automation*, May 2012.

[20] Berthold K. P. Horn and Brian G. Schunck. Determining optical flow. *Artificial Intelligence*, 17:185–203, 1981.

[21] Larry Matthies, Mark Maimone, Andrew Johnson, Yang Cheng, Reg Willson, Carolos Villalpando, Steve Goldberg, Andres Huertas, Andrew Stein, and Anelia Angelova. Computer vision on mars. *International Journal of Computer Vision*, 74:67–92, 2007.

[22] Michael Gewecke and Peter Schlegel. The vibrations of the antenna and their significance for flight control in the blow fly *Calliphora erythrocephala*. *Journal of Comparative Physiology A: Neuroethology, Sensory, Neural, and Behavioral Physiology*, 67:325–362, 1970. 10.1007/BF00340955.

[23] J. C. Kaimal and J. J. Finnigan. *Atmospheric boundary layer flows: Their structure and measurement*. Oxford University Press, 1994.

[24] Dietrich Burkhardt and Michael Gewecke. Mechanoreception in *Arthropoda*: the chain from stimulus to behavioral pattern. *Cold Spring Harbor Symposium on Quantitative Biology*, 30:601–614, 1965.

[25] Petros Argyrakis, Alister Hamilton, Barbara Webb, Yaxiong Zhang, Theophile Gonos, and Rebecca Cheung. Fabrication and characterization of a wind sensor for integration with a neuron circuit. *Microelectron. Eng.*, 84(5-8):1749–1753, May 2007.

[26] Mahdi M. Sadeghi, Rebecca L. Peterson, and Khalil Najafi. Hair-based sensors for micro-autonomous systems. In Thomas George, M. Saif Islam, and Achyut Dutta, editors, *Proc. SPIE 8373, Micro- and Nanotechnology Sensors, Systems, and Applications IV, 83731L*, volume 8373, page 83731L. SPIE, 2012.

[27] Pratheev S. Sreetharan, John P. Whitney, Mark D. Strauss, and Robert J. Wood. Monolithic fabrication of millimeter-scale machines. *Journal of Micromechanics and Microengineering*, 22(5):055027, 2012.

[28] M. Karpelson, Gu-Yeon Wei, and R. J. Wood. A review of actuation and power electronics options for flapping-wing robotic insects. In *Proc. IEEE Int. Conf. Robotics and Automation ICRA 2008*, pages 779–786, 2008.

[29] Akira Mamiya, Andrew D. Straw, Egill Tómasson, and Michael H. Dickinson. Active and passive antennal movements during visually guided steering in flying drosophila. *The Journal of Neuroscience*, 31(18):6900–6914, 2011.

[30] Matthew Keennon, Karl Klingebiel, Henry Won, and Alexander Andriukov. Development of the nano hummingbird: A tailless flapping wing micro air vehicle. In *AIAA Aerospace Sciences Meeting*, 2012.

[31] Kevin Y. Ma, Samuel M. Felton, and Robert J. Wood. Design, fabrication, and modeling of the split actuator microrobotic bee. In *Proceedings of the IEEE Int Robotics and Automation Conference*, 2012.